Inductive De-fluxing of Superconducting Quantum Interference Devices

Andrei N. Matlashov[1], Vasili K. Semenov[2*], William H. Anderson[3]

[1]Center for Axion and Precision Physics, IBS, Daejeon 34141, South Korea
[2]Department of Physics and Astronomy, Stony Brook University, Stony Brook, NY 11794-3800
[3]Imagion Biosystems, LLC, Albuquerque, NM 87106, USA

*E-mail: vasili.semenov@stonybrook.edu

Abstract— **Magnetic flux trapping is a serious problem in both low-temperature (LTS) and high-temperature (HTS) thin-film superconductive quantum interference devices (SQUIDs) and Josephson junction circuits. Trapped vortices in Josephson junctions can significantly degrade SQUID properties or even make them completely non-functional. Vortices can be trapped in superconducting films during the cooling process or can be caused by transient currents during current switching, electrostatic discharges through cable connections, etc. Unavoidable flux trapping happens in SQUIDs when a strong external field is applied. It can be a magnetization field in the case of superparamagnetic relaxation measurements (SPMR) or a pre-polarization field in the case of ultra-low field magnetic resonance imaging (ULF MRI), when an unshielded thin-film SQUID-based gradiometer is used. SQUID sensors stop working after being exposed to magnetic fields of only a few Gauss in strength. The most common way to remove frozen vortices is heating up a SQUID chip above its critical temperature which removes trapped fluxes and returns a SQUID to a normal operation. However, heating up a whole chip is usually too slow, is not reliably repeatable and dissipates too much energy. Earlier, we proposed a new alternative method for fast removal of trapped vortices in superconducting thin films by applying sinusoidal decaying magnetic field in an orthogonal direction. We called this method an alternating current or AC de-fluxing technique. In this paper we compile results obtained using planar thin-film LTS SQUID gradiometers and thin-film HTS SQUID magnetometers with bi-crystal Josephson junctions. This new inductive AC de-fluxing technique is much faster than a conventional thermal cycling and dissipates significantly less energy. The technique was successfully tested with multiple LTS and HTS SQUID sensors. Finally, we discuss a possible mechanism to explain the observed inductive de-fluxing effects.** We propose vortex-antivortex annihilation as a plausible mechanism explaining the observed inductive de-fluxing effects.

Keywords **- Magnetic flux, flux trapping, de-fluxing, thin film, Josephson junction, superconducting quantum interference device, SQUID, vortex, antivortex.**

I.   INTRODUCTION

Since their first introduction in 1970 [1], SQUID-based measuring instruments appear to be the most sensitive measurement tool for biomagnetism and fundamental physics as well as for many other applications. In some areas, SQUIDs cannot be replaced by any other type of magnetic field sensors. The revolutionary step in SQUID systems design was the

development of integrated thin-film sensors. These integrated sensors include both a SQUID and a pick-up coil or gradiometer coils deposited on a single substrate. They became unbeatable leaders in terms of high field resolution, high balance levels in the case of gradiometers, and they have high reliability and reproducibility (see, for example, [2], [3] and [4]).

Commercial all-thin-film magnetometers and gradiometers cover practically all application areas, except those where Josephson junctions are unavoidably exposed to strong external magnetic fields and trap magnetic fluxes, thus significantly decreasing junction critical currents. For instance, such exposure happens in the cases of ultra-low field magnetic resonance imaging (ULF MRI) [5] and super-paramagnetic relaxometry (SPMR) [6] using thin-film planar gradiometers. Such gradiometers consist of SQUIDs and pick-up coils deposited on the same substrate in close proximity to each other. As a result, SQUIDs unavoidably trap magnetic fluxes and stop working. Thermal cycling can provide de-fluxing, but it takes too long time while a few millisecond SQUID recovery time is expected after the external field is turned off.

In recent publications, we presented a new inductive de-fluxing technique that is based on applying strong decaying sinusoidal alternating current (AC) magnetic pulses with a few kilohertz carrier frequency [7, 8]. No obvious dependence of the de-fluxing efficiency on the carrier frequency or pulse duration has been detected. This technique was thoroughly tested with commercial thin-film niobium planar first-order G136 gradiometers [4] used for SPMR measurements. In our experiments, four gradiometers were exposed to up to 10 mT magnetizing DC field oriented perpendicular to their pick-up areas, causing them to stop working immediately when the field was applied. One short AC de-fluxing pulse made all four gradiometers completely operational again.

The inductive AC de-fluxing technique was also successfully tested with commercial SQ180, SQ300, SQ600, SQ2600 LTS SQUID sensors and MAG8 magnetometer from Star Cryoelectronics and CE2blue sensor and SM7.5 magnetometer from Supracon AG.

Another important application of the inductive AC de-fluxing technique can be for HTS SQUIDs. The discovery of high-temperature superconductivity in 1986 generated considerable interest in making SQUIDs working at liquid nitrogen temperature, $T = 77$ K. This would allow replacement of liquid helium by liquid nitrogen which is much cheaper and easy to use. The first successful and reliable HTS thin film Josephson junctions and SQUIDs were fabricated from yttrium cuprate $YBa_2Cu_3O_{7-\delta}$ (YBCO) deposited on bi-crystal epitaxial substrates. This type of HTS SQUIDs we used in our tests.

Unfortunately, HTS SQUIDs cooled in the Earth's magnetic field may trap flux that decreases a Josephson junction's critical current [9]. By applying a strong enough sinusoidal decaying magnetic field in the direction orthogonal to the pickup plane it was possible to increase the critical current to its normal value. The inductive AC de-fluxing technique worked very well with three commercial YBCO SQUID magnetometers made on 10×10 mm^2 bi-crystal substrates. In our experiments HTS SQUIDs de-fluxing reproducibility was 100%.

The energy dissipated by inductive de-fluxing pulses is significantly lower than that dissipated during conventional thermal cycling. This technique can be used with multiple

SQUID sensors installed in dilution refrigerators, for instance, in the neutron electric dipole moment (nEDM) experiments [10]. Hundreds SQUID sensors can be de-fluxed at once.

II. EXPERIMENTAL SETUPS

Each experimental setup depends on the size and shape of every LTS or HTS SQUID sensor under investigation. Electronic components such as capacitors and inductive coils have different properties varying with decreasing temperature so AC de-fluxing setups for HTS and LTS SQUIDs should be designed differently. Pure copper has significantly smaller electric resistivity at liquid helium temperature, T = 4.2 K, than at liquid nitrogen temperature, T = 77 K. This is why AC de-fluxing coils for LTS sensors can be wound using very fine copper wire to help minimize their size. As an LTS setup example, we describe the de-fluxing schematic design for niobium thin-film planar G136 gradiometers from Star Cryoelectronics [4]. The operational principle stays the same for any other LTS SQUID sensors but de-fluxing coils parameters must be individually optimized.

This LTS experimental setup was specifically designed for a four-channel system built for SPMR measurements. Four G136 first-order planar gradiometers were placed in parallel to each other in one plane (Figure 1) inside a biomagnetic fiberglass cryostat (Model 607 from BTi) and positioned slightly above the cryostat's tail bottom. The gradiometers were connected to the commercial room-temperature SQUID electronics PCI-1800 from Star Cryoelectronics [11]. Four blue discs schematically show shapes and positions of the four individual AC de-fluxing coils.
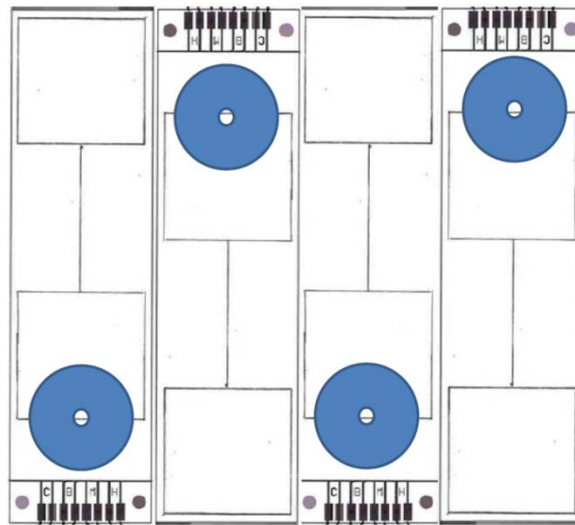

Fig.1. Four G136 gradiometers placed in parallel in one plane near the bottom of a biomagnetic fiberglass cryostat model 607 from BTi; the four blue discs illustrate the shape and size of the de-fluxing coils placed right above the DC SQUIDs.

Each first-order planar gradiometer consists of a dc SQUID and gradiometer pick-up coils deposited on a 12×48 mm^2 silicon substrate. The substrate is glued and bonded to a 16×58 mm^2 printed-circuit board, and is covered by a fiberglass protection cup. The four

de-fluxing coils (L_1 to L_4) are connected in series with the capacitor C_0 to form an LC-resonator with resonant frequency $f_0 = 12.9$ kHz (Figure 2). One de-fluxing pulse applied to L_5 is sufficient to restore all four gradiometers simultaneously.

Coil L_5 is coaxially placed on top of coil L_1 and is used to generate the excitation AC pulse from external electronics. All coils, $L_1 - L_5$, have a pancake shape with 15 mm outer diameters (OD). The AC current pulse I_{AC} is applied to coil L_5 and stimulates ringing of the LC-resonator. The excitation AC current is measured using a 1 Ohm reference resistor. A one-turn 10 mm diameter coil L_6 is coaxially placed directly under coil L_4 and used to
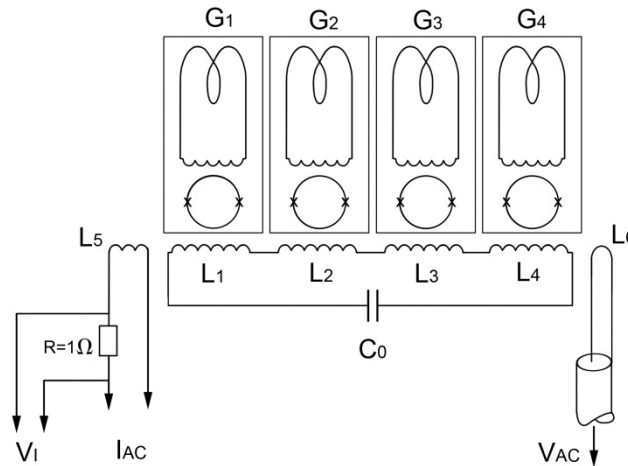

Fig.2. Schematic of the AC de-fluxing setup: a DC SQUID and pick-up coils are patterned on a 12×48 mm² silicon substrate; AC de-fluxing magnetic field is generated by $L_1 - L_4$; together with C_0 they form an LC-resonator with $Q \approx 100$ at $f_0 = 12.9$ kHz; AC current pulse in L_5 rings the LC-resonator; one-turn Ø10 mm L_6 is used to read out the strength of the AC de-fluxing magnetic field.
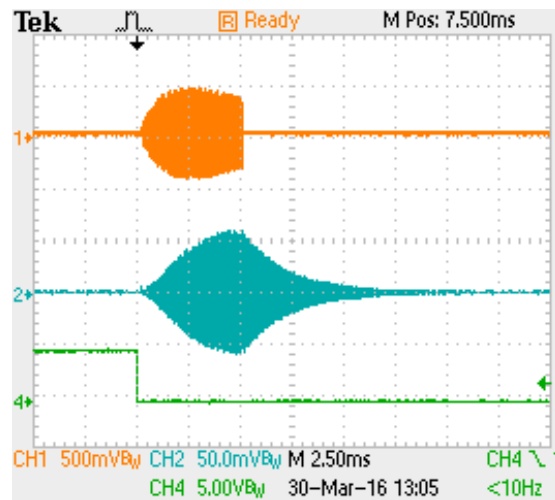

Fig.3. Oscilloscope screenshot: orange – AC current pulse in coil L_5 measured on 1 Ohm reference resistor; blue – AC output voltage from coil L_6; green – TTL control signal that turns off the magnetizing field and starts the AC de-fluxing signal (TTL: transistor-transistor logic).

read out the AC voltage that allows calculating the de-fluxing magnetic field in its plane.

Figure 3 shows AC current pulse in coil L_5 (orange) and AC output voltage (blue)

from coil L_6. The AC excitation current pulse is applied to coil L_5 for 5 ms. It's carrier frequency is tuned close to the resonance frequency of the LC-resonator, $f_0 = 12.9$ kHz. The output voltage of approximately 100 mV from coil L_6 on this screenshot corresponds to a 16 mT (peak-to-peak) AC de-fluxing magnetic field.

The experimental setup principle of operation for HTS SQUID magnetometers is the same as for LTS SQUIDs, although the schematics and coils geometry are different. In the HTS setup we used two significantly larger de-fluxing coils with OD = 40 mm, inner diameter (ID) = 20 mm, height (H) = 10 mm and inductance $L = 4$ mH. Such dimensions
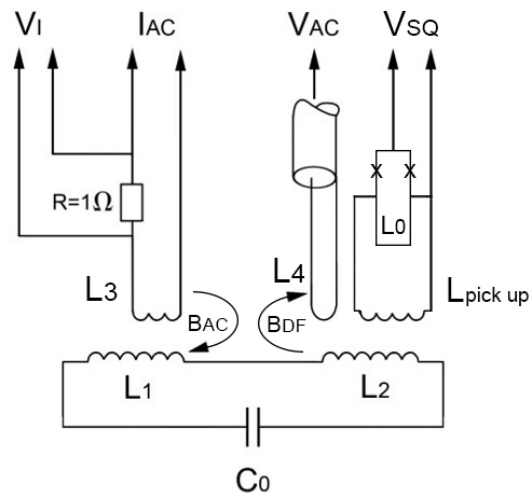

Fig.4. Schematic of the AC de-fluxing setup: a thin film YBCO magnetometer consists of a bi-crystal dc SQUID with loop inductance L_0 that directly coupled with a washer shaped pick-up loop $L_{PICK-UP}$; AC de-fluxing magnetic field B_{DF} is generated by coil L_2; coils L_1 and L_2 together with a capacitor C_0 form an LC-resonator; AC current pulse in L_3 rings the LC-resonator at resonance frequency $f_0 = 5.9$ kHz; one-turn L_4 is used to read out the strength of the AC de-fluxing magnetic field.

allowed positioning a whole HTS SQUID magnetometer coaxially inside coil L_2. In this situation its YBCO thin film pattern 10×10 mm size is completely immersed in the sufficiently uniform de-magnetizing field. The bi-crystal chip is glued to a 2 mm thick round shaped printed circuit board and bonded to it. The chip is covered with a round shaped protection cap. The magnetometer sensor is shaped as a button 19 mm in diameter and 4 mm in height.

We have tested AC de-fluxing operation using three YBCO bi-crystal dc SQUIDs. The detailed description of such SQUID magnetometers and their parameters can be found in reference material [12]. Figure 4 shows schematic diagram of the setup. The LC-resonator consists of coils L_1, L_2 and capacitor C_0. A short sinusoidal current pulse in L_3 that is inductively coupled with L_1 rings the LC-resonator at resonance frequency $f_0 = 5.9$ kHz. One-turn L_4 is used to read out the strength of the AC de-fluxing magnetic field with sensitivity 1.3 V/T. It was placed right on the top of the magnetometer enclosure.

Figure 5 shows signals viewed on an oscilloscope during the magnetizing and following de-fluxing of the HTS magnetometer placed inside coil L_2. Channel 1 (orange) shows the voltage on a 10 mOhm reference resistor installed in series with an external

magnetizing coil. The 64 mV output voltage corresponds to 6.4 A current and about 7.5 mT magnetizing field oriented orthogonally to the magnetometer pick-up loop. The signal from read-out coil L_4 is amplified with a gain of 100 and connected to channel 2 (blue). Its maximum peak-to-peak voltage of 1.38 V corresponds to 10 mT de-fluxing field amplitude. Channel 3 (magenta) shows the sinusoidal ringing current on a 1 Ohm reference resistor and channel 4 (green) is used for triggering.
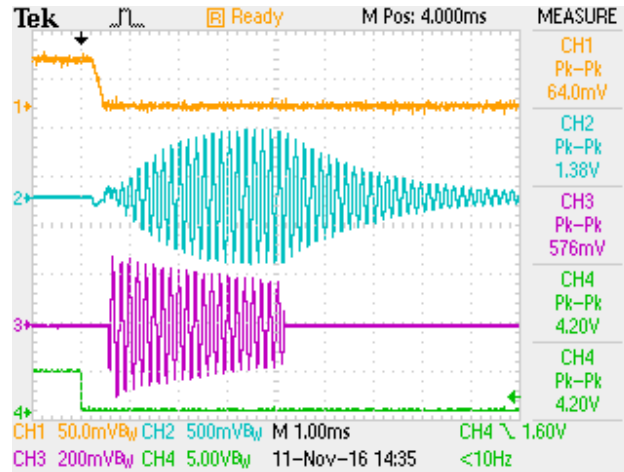

Fig.5. Oscilloscope screenshot: orange curve – external magnetizing pulse 7.5 mT; blue decaying signal – AC output voltage from coil L_4 corresponding to about 10 mT (peak-to-peak) field; magenta curve – AC current pulse in coil L_3 measured on 1 Ohm reference resistor; green signal – TTL control signal that turns off the magnetizing field and starts the AC de-fluxing signal.

For evaluation of the AC de-fluxing technique applied to HTS magnetometers, we used a helium fiberglass cryostat with a 150 mm long tail designed for biomagnetic applications. It was filled with liquid nitrogen and installed inside a single-layer magnetically shielded room (MSR) with a shielding factor $S_1 = 40$ at 1 Hz. All AC de-fluxing components and the HTS SQUID magnetometer were placed on a cryogenic probe in the cryostat tail and oriented in the horizontal direction. The room temperature coil generated a magnetizing field orthogonal to the magnetometer and was calibrated using a commercial AMR magnetometer.

III. EXPERIMENTATION

In the LTS experimental setup, the fiberglass cryostat was positioned in a vertical direction along the axis of a square-shaped magnetizing Helmholtz coil with a side length of 80 cm. The cryostat tail was placed a little bit above the coil geometrical center. The uniform magnetizing field was oriented perpendicular to the gradiometers plane. The whole setup was not magnetically shielded.

All four planar gradiometers became non-functional and the voltage-flux signals, also called the $V(\Phi)$ curves, practically disappeared after the DC magnetizing field >2 mT was

applied. To avoid influence of the SQUID electronics on SQUID sensors during the de-fluxing process we set all SQUID biases from the readout electronics to zero.

One AC de-fluxing pulse was applied immediately after the magnetizing field was turned off, and 40 ms after the de-fluxing pulse the SQUID control software automatically began searching for the working currents (I_W) of all four gradiometers. The working current corresponds to the first maximal amplitude of the voltage-flux signal as the bias current was increased from zero. The working currents of G136 gradiometers are normally slightly above their upper critical currents, $I_W \approx 1.05 \times I_C$. This measurement procedure was repeated 10 times for each of 30 amplitudes of the applied AC de-fluxing fields. Figure 6 shows the dependence of the working currents vs. the de-fluxing field strength (left graph) and the working currents vs. the voltage-flux signal amplitudes 2D distribution (right graph) for the first gradiometer G_1. This gradiometer is coupled to the de-fluxing coil L_1 and also parasitically to the ringing excitation coil L_5. When the AC de-fluxing magnetic field strength was small, the working currents never reached the maximal working current value $I_{Wmax} = 27.3$ µA. With increasing strength of the de-fluxing magnetic field, the working currents range moves up toward the maximal value that corresponds to a truly
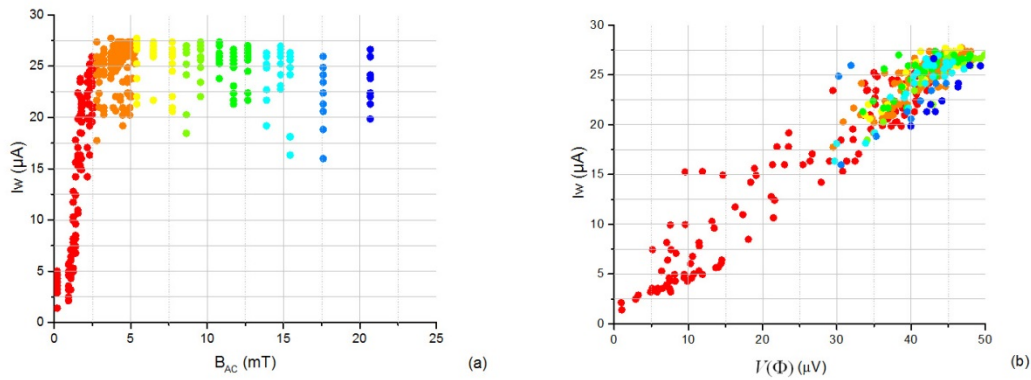

Fig. 6. (a) Dependence of working currents I_W (µA) vs. the de-fluxing field B_{AC} (mT) for G_1; (b) Working currents vs. $V(\Phi)$ 2D distribution amplitude. G_1 is coupled to the de-fluxing coil and also parasitically to the ringing excitation coil. Rainbow colors correspond to B_{AC} amplitudes.
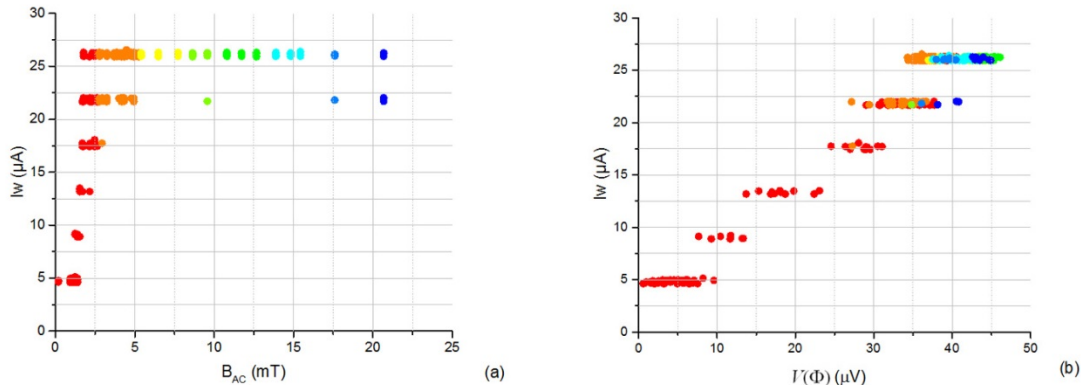

Fig. 7. (a) Dependence of working currents I_W (µA) vs. the de-fluxing field B_{AC} (mT) for G_2; (b): Working currents and $V(\Phi)$ amplitude. G_2 is coupled only to the de-fluxing coil.

thermally cycled SQUID. At the de-fluxing field strength of >4 mT, the SQUID becomes fully functional with almost maximal $V(\Phi)$ amplitude and low intrinsic noise level after each de-fluxing pulse.

At a high enough strength of the AC de-fluxing magnetic field, all four gradiometers became completely functional shortly after each pulse. In our particular settings the dead time after the de-fluxing pulse was set to 40 ms, at which point the de-fluxing magnetic field decays below the level of interference with the SQUIDs. This dead time can be significantly decreased with higher AC frequency or lower Q-factor of the LC-resonator. In our experiments we were able to decrease it to below 10 ms.

De-fluxing graphs for the first gradiometer look significantly different from the de-fluxing graphs for the three other gradiometers. Figure 7 shows the dependence of working currents vs. the de-fluxing field strength (left graph) and the working currents vs. the voltage-flux signal amplitudes 2D distribution (right graph) for the second gradiometer (G_2). The third and the fourth gradiometers $(G_3$ and $G_4)$ behaved virtually identically to the second one. All three gradiometers exhibit six discrete working current levels differing by 4.3 µA that cannot be explained at this time. The results were collected from all gradiometers in identical measuring conditions using the same hardware and software.
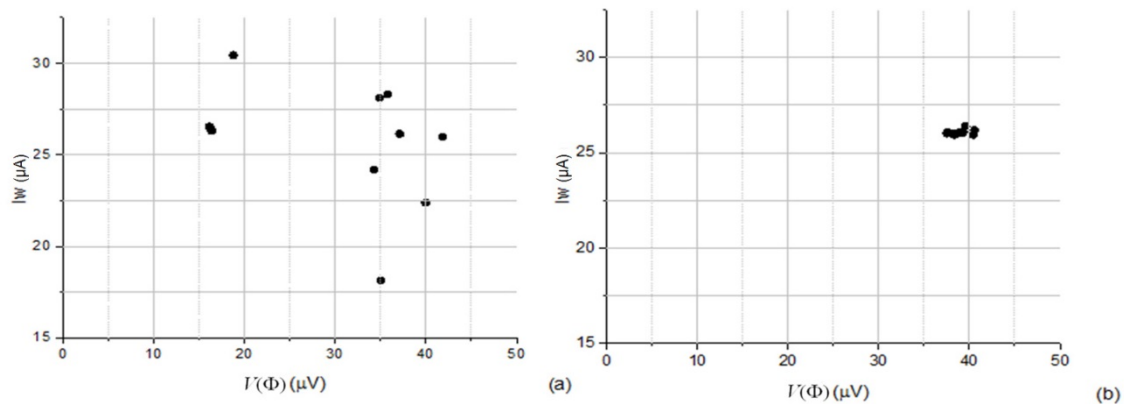

Fig. 8. (a) Working current I_W (µA) vs. $V(\Phi)$ amplitude scattering when G_2 bias current was not zeroed; (b) G_2 bias current zeroed during magnetization and de-fluxing times.

The only obvious difference between G_1 and the other three gradiometers is that G_1 was coupled to the pulse excitation coil L_5, which stayed connected to room-temperature circuits. This might cause additional noise that therefore blurs or destroys the discrete behavior of the SQUID during the de-fluxing process.

The discrete working current levels also disappear, and all I_W vs. B_{AC} and I_W vs. $V(\Phi)$ plots look similar to the first gradiometer on Figure 6, if bias currents coming to SQUIDs from the electronics are not zeroed during the de-fluxing process. Figure 8 shows scattering ranges of the working current I_W (µA) and $V(\Phi)$ for the second gradiometer G_2 when its bias current was not zeroed (left graph) and zeroed (right graph) during de-fluxing time. Figure 8 (b) illustrates very narrow variations of the working current and the $V(\Phi)$ amplitudes in the case when the bias current was zeroed during de-fluxing pulses.

It is also important to investigate reproducibility of the AC de-fluxing method for many repeated measurements. Figure 9 shows working currents of G_2 across one hundred de-fluxing pulses while zeroing its bias current. The measured working currents are distributed between 25.9 µA and 26.7 µA with three distinguishable levels. The gap between these levels is about 0.4 µA and it is probably caused by the bias current coarse automatic adjustment steps used in our experiments. The right plot shows the 2D distribution of the V(Φ) amplitudes and the working currents.

The AC de-fluxing technique is not fully equivalent to thermal cycling and it also works differently for different SQUID sensors. Some vortices may be still trapped in niobium strips and could increase $1/f$ noise. Nevertheless, we did not see any significant $1/f$ noise increase in the commercial LTS G136 gradiometers after AC de-fluxing.
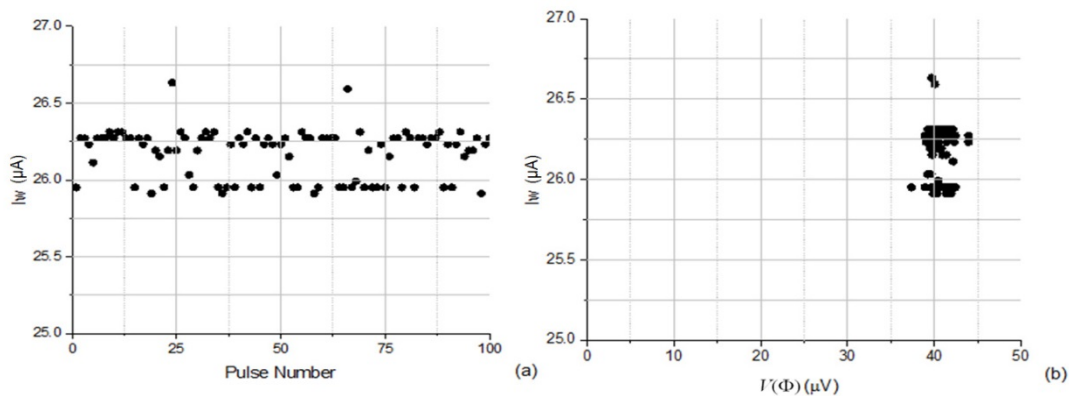

Fig. 9. Reproducibility of I_W and $V(\Phi)$ amplitude for G_2 when its bias current was zeroed during de-fluxing time: (a) working currents I_W (µA) vs. de-fluxing pulse number; (b) 2D scattering of the working currents I_W (µA) and $V(\Phi)$ amplitude within one hundred AC de-fluxing pulses.

As shown above, the experimental setup for HTS SQUIDs was quite different from that used for LTS. We tested the AC de-fluxing technique using three identically designed YBCO SQUID magnetometers inside a single-layer MSR with an internal residual DC magnetic field less than 10 µT[1]. HTS magnetometers instantly became non-functional when a magnetizing field >0.5 mT was applied using an external coil. The HTS magnetometer used throughout the testing had a working bias current of $I_B = 21.2$ µA that was measured after the magnetometer was slowly cooled down inside the MSR. After magnetizing using 0.5 – 10 mT fields, its critical current decreased below 2 µA and the voltage-flux signals could barely be seen on an oscilloscope. This behavior seemed to be independent from varying the strength or duration of the applied external field. Even after applying 10 mT field, one can still see tiny voltage-flux signals at a few µA bias current.

During AC de-fluxing periods we set all the signals coming to the magnetometer from the SQUID electronics to zero. The AC de-fluxing procedures used with the HTS SQUIDs were very similar to what was described above for the LTS SQUIDs. Figure 10

---

[1] We tested magnetometers, because gradiometers weren't available, however this shouldn't make any difference, as follows from the model presented below.

shows the dependence of the working currents vs. the de-fluxing field strength for 1 mT (left graph) and 10 mT (right graph) magnetizing fields.

In the case of a 1 mT magnetizing field, when the AC de-fluxing magnetic field strength was below approximately 2.5 mT the working currents never reached the maximal value of $I_{\text{Wmax}} = 21.2$ µA. With increasing strength of the de-fluxing magnetic field, the working currents range moved up toward the maximal value equal that of a thermally cycled SQUID. At de-fluxing field strength above 3 mT, the SQUID magnetometer became fully functional with maximal $V(\Phi)$ amplitude. Such a magnetometer can be used for measurements without fine tuning of the working current. The magnetometer needed more than 12 mT de-fluxing field after it was magnetized by 10 mT external DC field.

The inductive de-fluxing technique works very well for returning the bi-crystal junction's critical currents in HTS SQUIDs back to normal. Nevertheless, it didn't decrease its low-frequency $1/f$ noise. The AC biasing technique was not able to eliminate such noise. It probably means that a mechanism of the low-frequency $1/f$ noise is associated with leftover vortices still trapped in YBCO film away from the junctions.
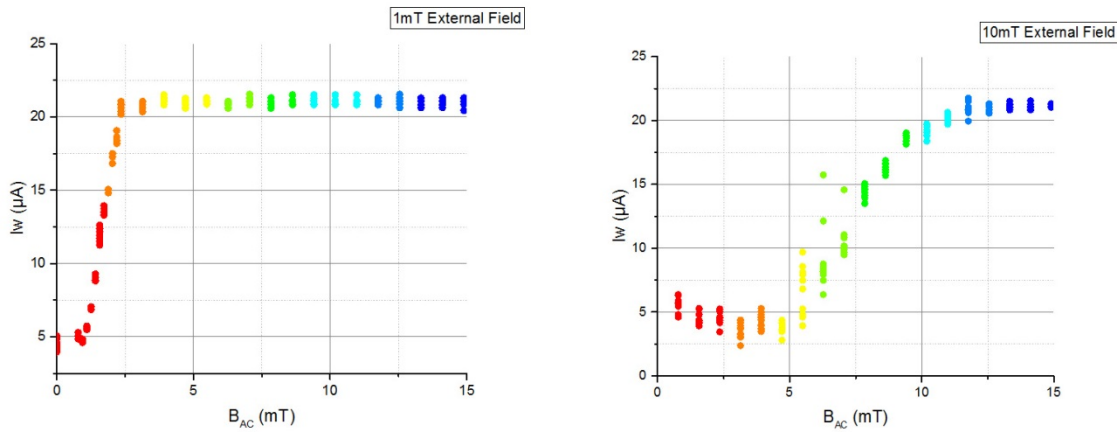

Fig.10. Dependence of working currents I_W (µA) vs. the de-fluxing field B_{AC} (mT) for HTS SQUIDs with bi-crystal Josephson junctions magnetized by 1 mT (left) and 10 mT (right) external magnetic field before applying one de-fluxing pulse.

The AC de-fluxing technique has extremely low energy dissipation. In the case of LTS de-fluxing of G136 gradiometers, each de-fluxing coil has inductance of 2×10^{-4} H. During the decaying process, it dissipates all energy stored at the highest strength of the de-fluxing magnetic field. The total magnetic flux measured by the one-turn read-out coil L_6 is about 2×10^{-6} Wb using a 10 mT de-fluxing field. Thus, the total stored energy in each coil is about 10^{-8} J per pulse. In comparison, each conventional thermal cycle of G136 gradiometer dissipates about 0.5 J of energy and takes about 1 second.

IV. VORTEX MODEL

The critical fields of strip-shaped superconductor films are inversely proportional to the second power of their widths (see, for example [13]), and it is vanishingly small for wide

strips. In very thin films and in films made of Type II superconductors, the field penetrates superconductors as quantized vortices [14]. Their properties are quite different from the
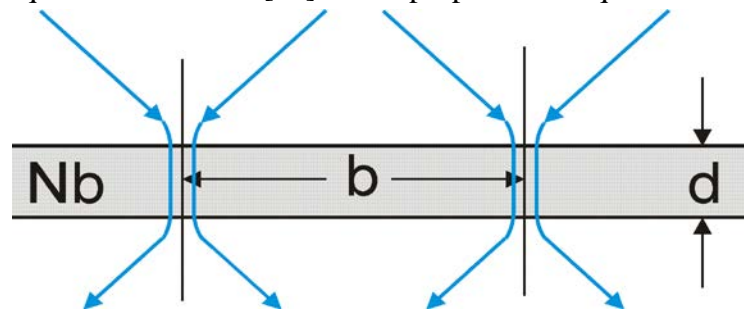

Fig.11. Interaction of vortices in thin superconductor film: Vortex kernels practically do not interact at distances b much longer than penetration length λ. The vortices interact only via their stray magnetic fields located above and below the film.

well-known Abrikosov vortices existing in bulk superconductors [15]. According to Pearl [16], the field created by the vortex above and below the film plays an important role in thin films. In particular, the field induces surface current i, that at large distances b, falls off as $i \sim 1/b^2$ [17]. This current, in turn, is responsible for the long distance Lorentz force $\sim i \cdot \Phi_0$ that attracts vortices of opposite signs and repels vortices of same signs, Figure 11. Due to such long distance forces, Pearl's vortices could be organized into a regular grid. At large fields, the density of vortices n is directly proportional to the perpendicular component of the external field B:

$$n = B/\Phi_0. \tag{1}$$

The static vortex distribution corresponds to a balance of two forces. The external field forces vortices to enter the film via its edges, while the Lorentz force does not allow them to stay too close to each other. Ideally, n (eq. 1) would follow the changing applied field B. In reality, this motion is distorted by pinning forces associated with grain boundaries or other non-uniformities of the superconductor film [18]. In particular, some vortices may remain in the film even after the external field is dropped to zero. These residual vortices trapped in the film are able to spoil the SQUID operation. To restore the operation, we should remove the vortices. That is typically accomplished by heating the film above its critical temperature. Alternatively, one can investigate de-fluxing using a strong enough external decaying AC magnetic field.

At first glance, this is an almost impossible task. However, our straightforward experimental results demonstrated a very high (99+ %) probability of successful de-fluxing utilizing decaying AC magnetic fields. We propose a tentative explanation why this is possible. In fact, we should pay attention only to vortices frozen in the vicinity of Josephson junctions. Vortices frozen in passive films are only capable of biasing the measured flux in a SQUID loop, but unable to spoil the SQUID modulation depth.

Single layer high-T_c SQUIDs are easier to analyze. Figure 12 (a) shows a vicinity of a Josephson junction that could be described as a superconductor strip broken by the junc-
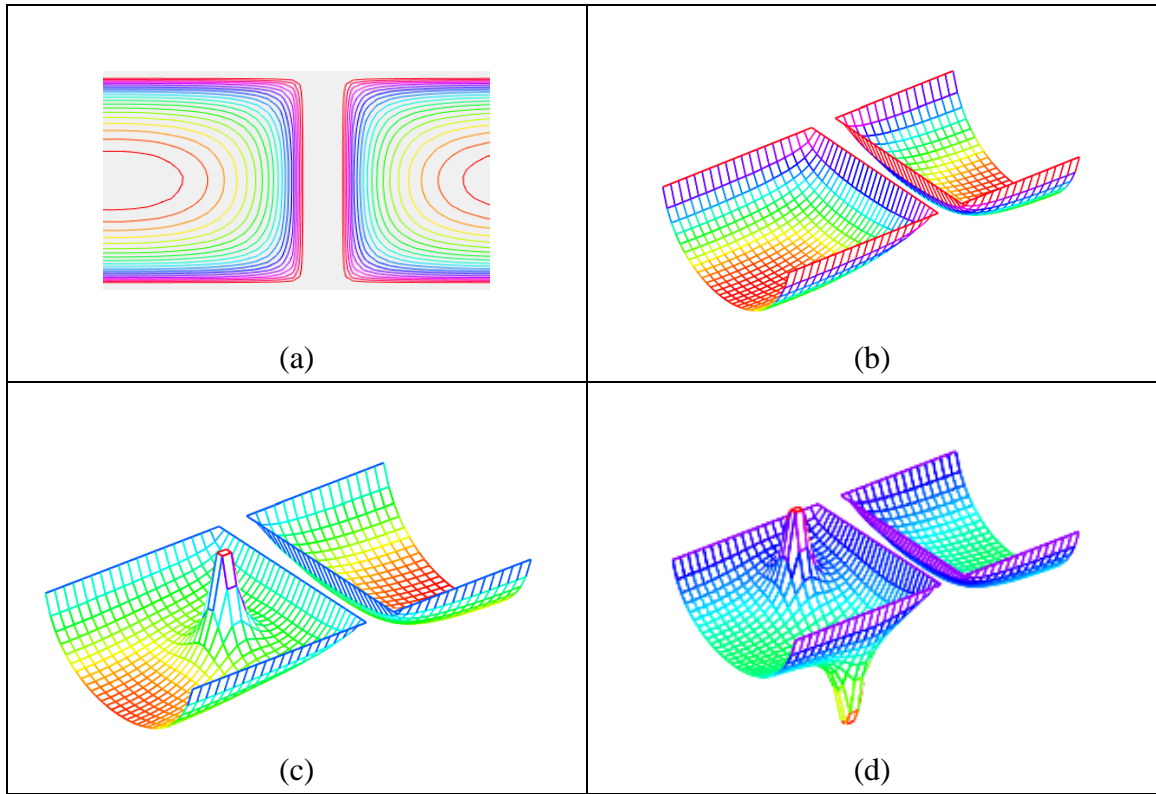
Fig. 12. Stream functions of vicinities of high-T_c Josephson junction with no (a,b), one (c) and two (d) vortices of opposite signs. A perpendicular magnetic field is applied to the junction.

tion into two pieces. A perpendicular magnetic field induces currents flowing via both pieces of the film. The intensities of the current are shown in the figure by stream functions. These functions [19], [20] are convenient because their gradients are proportional to the Lorentz force acting on vortices. For example, the steepness of the slope of stream functions shown in Fig. 12 (b) "visualizes" the forces that would be applied to vortices by the magnetic field. In Fig. 12 (c) one vortex entered the strip, moved out to its center and reduced the gradient of the slope. As a result, a lower Lorentz force would be insufficient to pull the next vortex into the film. Finally, Figure 12 (d) shows the film with one vortex and one "frozen" anti-vortex.

        Two-film (trilayer) low-T_c tunnel junctions are much more sensitive to the flux trapping. The parasitic impact of vortices strongly depends on the misalignment of vortices frozen in base and counterelectrode films. According to [16], two coaxial vortices, Figure 13 (a), reduce the effective junction area by a tiny value $\sim\xi^2$. At $T = 4$ K, the coherence length ξ of niobium films is about 0.1 µm. This is 40 fold lower than the diameter of circular-shaped Josephson junctions used in G136 gradiometers, D = 4 µm. The drop of the effective area becomes much larger ($\sim a^2$) if the vortices in the base and counter electrodes are misaligned, Figure 13 (b). The effective area is close to zero if only one electrode is punched by a vortex, Figure 13 (c).

    The de-fluxing mechanism could be described as follows. We do not know how to push the vortices shown in Fig. 13 from the junction. However, we can drop the field to zero, change its sign and start to increase it. In this case, the negative field will inject anti-vortices
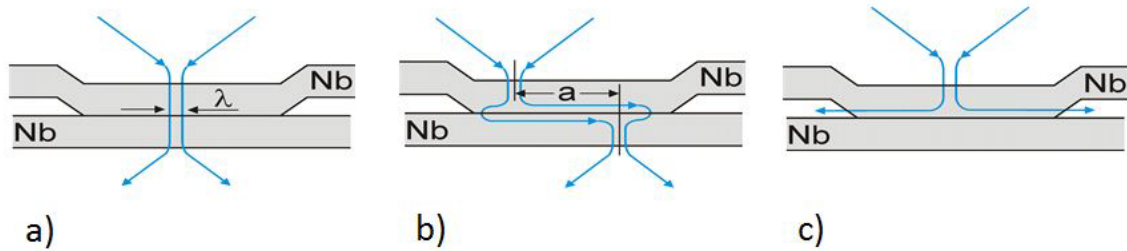
Fig. 13. Vortices in base and counter electrodes of Josephson junction. The vortices practically do not affect the junction if their misalignment is below penetration depth λ (a); their destruction effect is much larger at microscopic misalignments (b); it becomes catastrophic if only one of two electrodes is punched by a vortex.

via the film edges. These anti-vortices will expand into inner parts of the film due to the discussed earlier repulsion force. However, the expansion will be stronger due to the attraction forces between anti-vortices and trapped frozen vortices. Newly generated anti-vortices and pre-existing vortices annihilate each other when they are sufficiently close to each other. Due to the attraction of vortices with opposite signs, the negative external magnetic field required to annihilate all old vortices is lower than the initial positive magnetic field that placed the vortices into the junction. We propose vortex-antivortex annihilation as a plausible mechanism explaining the deletion of vortices from Josephson junctions using the inductive AC de-fluxing technique.

V. CONCLUSION

The thin-film LTS or HTS SQUIDs or Josephson junction circuits may trap magnetic flux and stop operating, particularly in the presence of an externally applied magnetic field. The new inductive AC de-fluxing technique described in this paper quickly returns SQUID sensors back to normal operation with significantly lower recovery time and energy dissipation than conventional thermal cycling. This technique is based on applying a strong enough sinusoidal decaying AC magnetic field in the Josephson junction areas. No obvious frequency or decaying pulse length dependencies have been observed. It was successfully tested with several different types of commercial thin-film SQUID sensors including thorough tests of G136 planar gradiometers used in SPMR measurements. Equidistant discrete working current levels after de-fluxing pulses were observed in G136 gradiometers. However, this is not the case when the G136 gradiometer stayed continuously coupled to room-temperature circuits. The inductive AC de-fluxing technique has been successfully applied to HTS SQUIDs with bi-crystal Josephson junctions. Thanks to the extremely low energy dissipation this de-fluxing technique can be used in dilution refrigerators. We propose a simple physical mechanism for explaining effectiveness of the inductive de-fluxing through the use of strong AC decaying magnetic fields.

REFERENCES

[1] J. E. Zimmerman, P. Thiene, and J. T. Harding, "Design and Operation of Stable rf-Biased Superconducting Point Contact Quantum Devices, and a Note on the Properties of Perfectly Clean Metal Contact." *J. Appl. Phys.*, **41**, 1572 (1970), DOI: http://dx.doi.org/10.1063/1.1659074.

[2] A. I. Ahonen, *et al.* "122-channel SQUID instrument for investigating the magnetic signals from the human brain." *Physica Scripta*, **T49**, 198–205 (1993), DOI: http://dx.doi.org/10.1088/0031-8949/1993/T49A/033.

[3] H. J R. Stolz, L. Fritzsch, and H.-G. Meyer, "LTS SQUID sensor with a new configuration", *Supercond. Sci. Technology*, **12**, 806–808 (1999), DOI: http://dx.doi.org/10.1088/0953-2048/12/11/334.

[4] Cantor R., Hall J., Matlashov A., Volegov P., "First-Order Planar SQUID Gradiometers with Long Baseline." *IEEE Trans. on Appl. Supercond.,* **17**, no.2, 672- 675 (2007), DOI: 10.1109/TASC.2007.898537.

[5] Vadim S. Zotev,. *et al.* "Microtesla MRI of the human brain combined with MEG." *J. of Magn. Reson.*, **194,** (1), 115-120 (2008), DOI: 10.1016/j.jmr.2008.06.007.

[6] E. Leyma P De Haro *et al.*,"Magnetic Relaxometry as applied to Sensitive Cancer Detection and Localization" *Biomed. Engineering – Biomed. Technik* **60**, No.5, 445–455 (2015), DOI 10.1515/bmt-2015-0053.

[7] A. N. Matlashov, V. K. Sem*enov, and W. H. Anderson, "SQUIDs de-*fluxing using a d*eca*ying AC magnetic field." *IEEE/CSC & ESAS SUPERCONDUCTIVITY NEWS FORUM*, July 2016, ST 519 (6pp), http://snf.ieeecsc.org/sites/ieeecsc.org/files/documents/snf/abstracts/NEWkeytermsMatlashovA_De-fluxing-AM-final_060416.pdf.

[8] A. N. Matlashov, V. K. Semenov, and W. H. Anderson, "AC de-fluxing of SQUIDs." ." *IEEE Trans. on Appl. Supercond.,* (2017) (in print) DOI: 10.1109/TASC.2017.2650902.

[9] A. H. Miklich *et al.* "Low-frequency excess noise in $YBa_2Cu_3O_{7-\delta}$ dc superconducting quantum interference device cooled in static magnetic fields." *Appl. Phys. Lett.*, **64**, (No. 25), 3494-3496 (1994), http://dx.doi.org/10.1063/1.111251.

[10] T. M. Ito, et al. 'Neutron Electric Dipole Moment Experiment at Los Alamos Ultra Cold Neutron Source.", fsnutown.phy.ornl.gov/fsnufiles/positionpapers/nEDM_at_LANL.pdf

[11] STAR Cryoelectronics: http://starcryo.com/pcsquid/.

[12] R. Cantor, L. Lee, M. Teepe, V. Vinetskiy, and J. Longo "Low-Noise, Single-Layer $YBa_2Cu_3O_{7-\delta}$ DC SQUID Magnetometer at 77K." ." *IEEE Trans. on Appl. Supercond.,* **5**, No. 2, 2927- 2930 (1995), DOI: 10.1109/77.403205.

[13] G. Stan, S. B. Field, and J.M. Martinis, "Critical field for complete vortex expulsion from narrow superconducting strips," *Phys. Rev.* Lett, **92**, No. 9, 097003 (2004).

[14] P.-G. De Gennes, *Superconductivity of metals and alloys*, vol. 86: WA Benjamin, New York, 1966.

[15] A. A. Abrikosov, "The magnetic properties of superconducting alloys," *J. of Phys. and Chem. of Solids,* vol. **2**, (1957).

[16] J. Pearl, "Structure of superconductive vortices near a metal-air interface," *J. Appl. Phys.,* **37**, 4139-41 (1966).

[17] C. Peroz and C. Villard, "Flux flow properties of niobium thin films in clean and dirty superconducting limits," *Physical Review B,* **72**, 014515 (2005).

[18] A. A. Golubov and M. Y. Kupriyanov, "Theoretical investigation of Josephson tunnel-junctions with spatially inhomogeneous superconducting electrodes," *J. Low Temp. Phys.,* **70**, 83-130 (1988).

[19] V.K Semenov, M.M Khapaev, "How moats protect superconductor films from flux trapping," *IEEE Trans. on Appl. Supercond,* **26**, 1300710 (2016).

[20] M. M. Khapaev, "Extraction of inductances of plane thin film superconducting circuits," *Supercond. Sci. Technol.*, 10, No. 6, 389–394 (1997).